First determination of the ^{8}Li valence neutron asymptotic normalization coefficient using the ^{7}Li(^{8}Li,^{7}Li)^{8}Li reaction

D. Howell,[1,2] B. Davids,[2] J. P. Greene,[3] R. Kanungo,[4] S. Mythili,[2] C. Ruiz,[2] G. Ruprecht,[2] and I. J. Thompson[5]
[1]*Department of Physics, Simon Fraser University, Burnaby, British Columbia, Canada*
[2]*TRIUMF, Vancouver, British Columbia, Canada*
[3]*Physics Division, Argonne National Laboratory, Argonne, Illinois 60439, USA*
[4]*Astronomy and Physics Department, Saint Mary's University, Halifax, Nova Scotia B3H 3C3, Canada*
[5]*Lawrence Livermore National Laboratory L-414, Livermore, California 94551, USA*
(Received 26 February 2013; revised manuscript received 3 June 2013; published 19 August 2013)

We report here a determination of the asymptotic normalization coefficient of the valence neutron in ^{8}Li from a measurement of the angular distribution of the ^{7}Li(^{8}Li,^{7}Li)^{8}Li reaction at 11 MeV. Using isospin symmetry the ^{8}B ANC has also been calculated and used to infer a value for $S_{17}(0)$ of 20.2 ± 4.4 eV b.

DOI: 10.1103/PhysRevC.88.025804 PACS number(s): 25.70.Hi, 26.20.−f, 26.65.+t, 21.10.Jx

I. INTRODUCTION

The rates of many solar fusion reactions are still quite uncertain. Excluding the hep reaction, the decay of ^{8}B produces the highest energy solar neutrinos measured by SNO and Super-Kamiokande [1]. ^{8}B is produced via the ^{7}Be$(p,\gamma)^{8}$B reaction from the third branch of the *pp* chains. Therefore, the predicted solar neutrino flux from the β^{+} decay of ^{8}B is proportional to the thermally averaged rate of the ^{7}Be$(p,\gamma)^{8}$B radiative capture reaction, which is the most poorly known of all reactions of the *pp* chains, contributing a ±7.5% uncertainty to the rate predictions for Super-Kamiokande and SNO [1]. The purpose of this study is to make an indirect measurement of $S_{17}(0)$, the zero energy astrophysical *S* factor describing the ^{7}Be$(p,\gamma)^{8}$B reaction, from the elastic transfer reaction ^{7}Li(^{8}Li,^{7}Li)^{8}Li.

$S_{17}(0)$ has previously been derived from measurements of radiative capture, Coulomb breakup, and transfer reactions. Radiative capture measurements have been performed at relative kinetic energies as low as 117 keV [2] to obtain values for $S_{17}(0)$, but have been limited by large uncertainties both experimentally and theoretically when extrapolating to solar energies. Recent experimental progress [3] has greatly reduced the experimental uncertainties, rendering the theoretical extrapolation error dominant. Even when the radiative capture data considered is limited to relative kinetic energies below 475 keV, the theoretical uncertainty determined from the spread in the results from extrapolating using different models amounts to ±6.7% [1]. This uncertainty is considerably larger than the ±2.8% precision with which the ^{8}B solar neutrino flux has been measured by Super-Kamiokande [4]. The advent of *ab initio* calculations of ^{7}Be + *p* radiative capture, elastic, and inelastic scattering reactions [5] promises to eventually reduce the theoretical uncertainty, provided the calculations accurately describe published [6] and planned elastic and inelastic scattering measurements.

Measurements of the Coulomb breakup of ^{8}B are subject to uncertainties due to $E2$ transitions and multiple photon exchange which limit the precision of the inferred *S* factors. They also suffer from the same extrapolation uncertainties as radiative capture measurements. In contrast, measurements of related heavy ion transfer reactions provide another method of inferring the *S* factor which, while subject to different systematic uncertainties, does not require extrapolation.

Previous measurements of the heavy ion transfer reactions ^{10}B(^{7}Be,^{8}B)^{9}Be [7] and ^{14}N(^{7}Be,^{8}B)^{13}C [8,9] resulted in a central value of $S_{17}(0)$ approximately 12% smaller than the recommendation of Ref. [1], which is based solely on radiative capture measurements. A measurement of the ^{13}C(^{7}Li,^{8}Li)^{12}C neutron transfer reaction [10] was also used to infer a value of $S_{17}(0)$ 15% smaller than the recommendation of Ref. [1]. Although the uncertainties of these measurements range from 10–15%, the apparent systematic difference merits further investigation.

The interference between elastic scattering and neutron transfer in the ^{7}Li(^{8}Li,^{7}Li)^{8}Li reaction produces characteristic oscillations in the differential cross section as a function of the scattering angle. From the analysis of the differential cross section the asymptotic normalization coefficient (ANC) for the valence neutron in ^{8}Li can be determined and used to derive the ^{8}B valence proton ANC, which may be used to infer $S_{17}(0)$. This is the novel approach taken here.

II. THEORY

A brief primer based on Ref. [11] of the theory used to extract ANCs within a distorted wave Born approximation (DWBA) framework is presented here. We consider the reaction

$$X + A \rightarrow Y + B, \tag{1}$$

where $X = Y + a$, $B = A + a$, and a is the transferred particle. The entrance channel ANC, $C^{X}_{Yal_X j_X}$, may be calculated from the single particle ANC, $b_{Yal_X j_X}$, and the spectroscopic factor, $S_{Yal_X j_X}$:

$$\left(C^{X}_{Yal_X j_X}\right)^2 = S_{Yal_X j_X} b^2_{Yal_X j_X}, \tag{2}$$

where j_X is the total angular momentum of particle a in the nucleus X, and l_X is the orbital angular momentum of the relative motion of particles Y and a in the bound state $X = (Ya)$.

By writing the ANC in this form the dependence of the calculated DWBA differential cross section on the geometry of the bound state wave function is significantly reduced [11]. To illustrate this, the differential cross section can be written as

$$\frac{d\sigma}{d\Omega} = \sum_{j_B j_X} \frac{\left(C^B_{Aal_B j_B}\right)^2}{b^2_{Aal_B j_B}} \frac{\left(C^X_{Yal_X j_X}\right)^2}{b^2_{Yal_X j_X}} \sigma^{DW}_{l_B j_B l_X j_X}. \quad (3)$$

For peripheral reactions, only values where $r_{Ya} > R_X$ and $r_{Aa} > R_B$ will contribute to the DWBA radial integrals, where r_{Ya} and r_{Aa} are the separations, and R_X and R_B represent the nuclear interaction radii between the constituents of both nuclei X and B. Therefore, each of the bound state wave functions entering the expression for the DWBA cross section $\sigma^{DW}_{l_B j_B l_X j_X}$ can be approximated by its asymptotic form, with the product of the single particle ANCs containing the only dependence on the geometry of the bound state potentials. Reparametrizing the differential cross section as

$$\frac{d\sigma}{d\Omega} = \sum_{j_B j_X} \left(C^B_{Aal_B j_B}\right)^2 \left(C^X_{Yal_X j_X}\right)^2 R_{l_B j_B l_X j_X}, \quad (4)$$

the factor

$$R_{l_B j_B l_X j_X} = \frac{\sigma^{DW}_{l_B j_B l_X j_X}}{b^2_{Aal_B j_B} b^2_{Yal_X j_X}} \quad (5)$$

contains all the dependence on the geometry of the bound state potentials. This results in the parametrization of the peripheral reaction differential cross section in terms of the ANCs of the initial and final states which are insensitive to the geometries of the bound state potentials [11].

For the specific case of the ^{7}Be$(p,\gamma)^8$B reaction, the numerical relationship between $S_{17}(0)$ and the ^{8}B ANCs can be expressed by the relationship [9,12]

$$S_{17}(0) = 38.6\left[C^2_{p_{1/2}}(^8B) + C^2_{p_{3/2}}(^8B)\right] \text{eV b fm}, \quad (6)$$

where $C_{p_{1/2}}(^8B) \equiv C^{^8B}_{^7Be\,p\,1\frac{1}{2}}$ and $C_{p_{3/2}}(^8B) \equiv C^{^8B}_{^7Be\,p\,1\frac{3}{2}}$.

III. EXPERIMENT

The benefit of studying the ^{7}Li(^{8}Li,^{7}Li)^{8}Li reaction is apparent upon examination of Eq. (3). The two ANC terms $C^B_{Aal_B j_B}$ and $C^X_{Yal_X j_X}$, as well as the single particle ANC terms $b_{Aal_B j_B}$ and $b_{Yal_X j_X}$, are identical for this reaction thereby simplifying the expression and reducing the associated uncertainties.

The experiment was performed using the TUDA (TRIUMF-U.K. Detector Array) chamber in the ISAC I facility at TRIUMF in Vancouver, BC, Canada. A ^{8}Li^{2+} beam at an energy of 11 MeV with an intensity of 9–16 $\times$ 10^6 s^{-1} was used. Two annular detectors were used; a LEDA detector and a *S*2 detector. The TUDA chamber was specifically designed for use with the Louvain-Edinburgh Detector Array [13] (LEDA), which consists of eight separate azimuthal sectors, each with 16 radial elements. This annular detector is 300 μm thick and its active area spans radii from 50 mm to 129.9 mm. The *S*2 is a double sided silicon strip detector consisting of a single

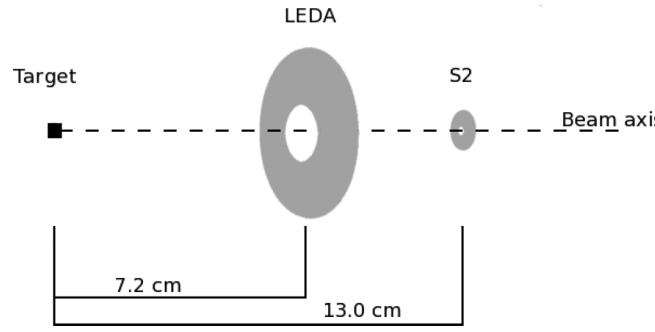

FIG. 1. Experimental setup of the LEDA and *S*2 detectors in the TUDA chamber.

element that is divided into 16 azimuthal sectors on the back side and 48 rings on the front. This 500 μm thick detector is considerably smaller than the LEDA, with its active area having an inner radius of 11.5 mm and an outer radius of 35 mm.

As shown in Fig. 1, within the TUDA chamber the LEDA and *S*2 detectors were mounted downstream from the target ladder at 72 mm and 130 mm, respectively, resulting in an angular coverage of 36–60 degrees for the LEDA and 5–15 degrees for the *S*2, both in the laboratory frame. The target used was 25 μg/cm^2 ^{7}LiF on a 10 μg/cm^2 carbon backing.

The presence of ^{19}F in the target gave rise to elastic scattering which was analyzed for calibration of both detectors. Comparing the absolute number of ^{8}Li elastically scattered from ^{19}F detected in the *S*2 detector between laboratory angles of 5 to 15 degrees an asymmetry was observed among the different sectors. This asymmetry is the result of a slight shift in the beam spot from the center of the detectors.

Using the data from ^{8}Li elastically scattered from ^{19}F, an analysis was performed to determine the displacement of each detector with respect to the beam axis. By varying the offset values and thus the correlated scattering angle the asymmetry was minimized and the beam offset was determined. The offset was found to be 0.05 $\pm$ 0.02 cm in the horizontal and 0.13 $\pm$ 0.01 cm in the vertical for the *S*2 detector. Due to the smaller statistics and reduced angular resolution in the LEDA its beam offset was difficult to determine precisely. Values obtained for the offset in the LEDA were 0.05 $\pm$ 0.05 cm in the horizontal and 0.10 $\pm$ 0.05 cm in the vertical. When comparing the offset LEDA data to the zero offset case no significant difference was observed. Therefore, the offset of the LEDA was set to zero in the analysis and the possible systematic errors due to this assumption are taken into account later.

IV. ANALYSIS

Reduction of the *S*2 data was performed via energy and time gates. An energy gate was placed on ring and sector energies ensuring agreement between the two channels within 3%. Further background reduction was achieved through timing cuts. Identification of various peaks in the TDC spectra was done by placing tight windows on known loci in the energy spectrum and assessing the corresponding peaks in the timing

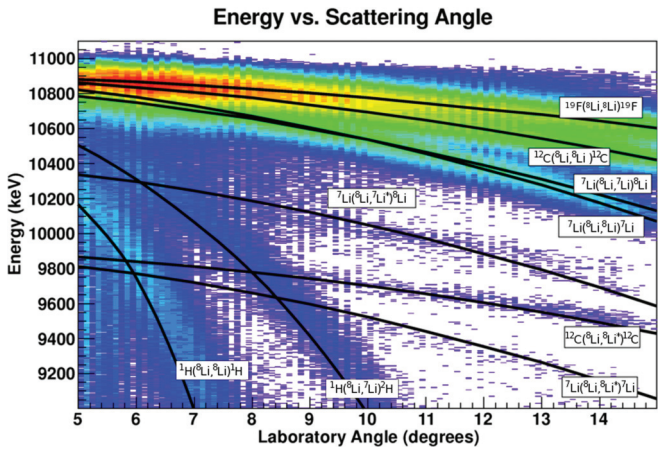

FIG. 2. (Color online) Identified loci in the *S*2 detector following background reduction. The theoretical kinematic loci shown in black, calculated using the well-measured masses of the reactants and products, have been corrected for energy loss in the target foil and the inactive layer at the front of the detector.

data. The data collected in the *S*2 following background reduction are shown in Fig. 2.

Even though the *S*2 detector subtended scattering angles between 5 and 15 degrees in the laboratory frame, the kinematics of the reactions made separating the elastic lithium locus from the stronger carbon and fluorine elastic loci impossible at angles below 9 degrees. From 9 degrees and up the lithium peak is sufficiently separated from the other peaks to perform a reliable multiple peak fit.

The components in the *S*2 fit include: a Gaussian for ^{8}Li and ^{7}Li from the ^{8}Li + ^{7}Li reaction, Gaussians for ^{8}Li elastic scattering from ^{12}C and ^{19}F, as well as linear and Gaussian backgrounds. The background Gaussian describes a small peak with a nearly uniform energy profile over the entire angular range which we attribute to elastic scattering from heavy contaminants; Fe, Te, Ba, and Pb were all known to be present in the target at trace levels. A typical multiple peak fit for the S2 data is shown in Fig. 3. The small excess of events above the fit at the low energy tail of the "Li Exchange" peak amounts to only 0.37% of the total ^{8}Li and ^{7}Li events from the ^{7}Li(^{8}Li,^{7}Li)^{8}Li reaction deduced from the fit. Imperfections in the fit just below and above the "Heavy Contaminants" peak are due to our assumption that elastic scattering from all the heavy contaminants can be represented by a single Gaussian. Actually the different contaminants produce individual peaks at slightly different energies, a fact we have neglected due to its irrelevance for the "Li Exchange" peak of interest. Excluding the "Heavy Contaminants" peak entirely from the fit changes the integral of the "Li Exchange" peak by only 1%. Hence these slight imperfections may safely be ignored.

As in the *S*2 detector, reaction loci in the LEDA detector were identified through kinematics rather than particle identification. ^{8}Li was detected with the LEDA detector in coincidence with ^{7}Li in the same detector, allowing us to easily separate these events from the background. Following the detection of an event consistent with ^{8}Li and a coincidence consistent with ^{7}Li, the individual energies were summed and compared to the expected total energy. The total energy

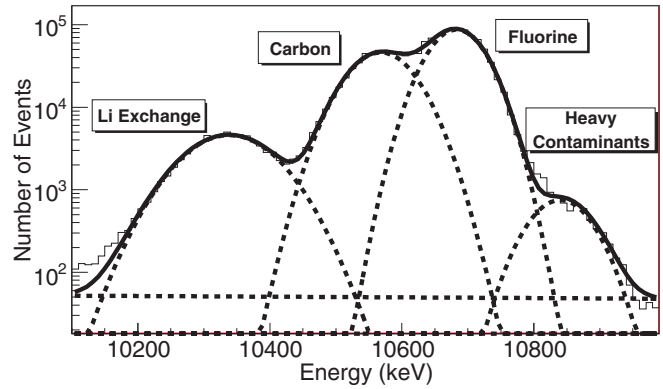

FIG. 3. (Color online) Data from the *S*2 detector between 12 and 13 degrees in the laboratory frame. The "Li Exchange" curve represents ^{8}Li and ^{7}Li from the elastic transfer reaction. The two curves labeled "Carbon" and "Fluorine" are ^{8}Li elastically scattered from ^{12}C and ^{19}F, respectively. The "Heavy Contaminants" peak is attributed to elastic scattering from trace heavy contaminants.

gate was corrected for energy loss through the target and dead layer of the LEDA detector based on SRIM energy loss calculations [14].

Figure 4 shows the detected coincidences of ^{8}Li and ^{7}Li in the LEDA detector. The top panel depicts the full range of detected coincidences, while the lower panels display projections at 41.0 and 50.5 degrees. Due to the coincidence requirement and the total energy gate the background in the LEDA was effectively reduced to zero.

For the *S*2 detector the large number of detected events resulted in small statistical errors of ±1.5% or less. The largest sources of error for the *S*2 are systematics. These errors arise from the extensive measures required to reduce the background and the difficulty in accurately performing multiple peak fits.

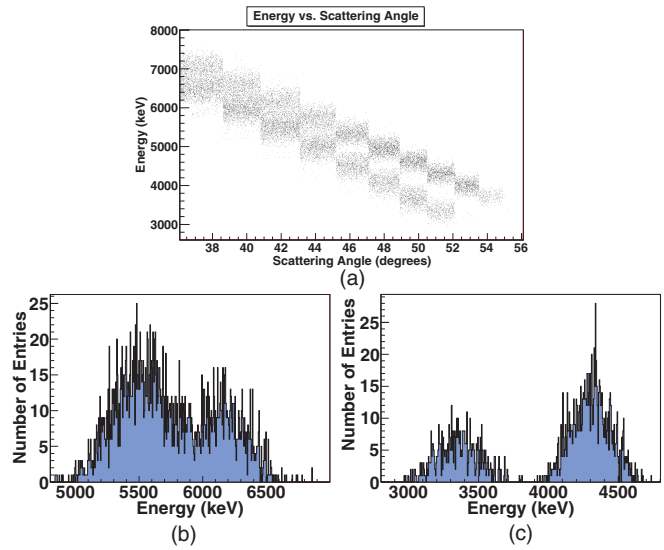

FIG. 4. (Color online) Coincidence events in the LEDA detector are shown in (a). The energy spectra of the 41.0–43.1 degree bin and the 50.5–52.0 degree bin are shown in (b) and (c), respectively. The higher energy locus represents ^{7}Li events and the lower energy locus represents ^{8}Li events.

TABLE I. Contributions to the point-to-point error for the data from the *S*2 and LEDA detectors. Total errors are the results of adding the statistical and systematic errors in quadrature.

Detector	Statistical error	Systematic error	Total
S2	0.3–1.5%	6.9%	6.9–7.1%
LEDA	2.8–6.2%	2.6%	3.8–6.7%

The estimated systematic errors due to background reduction cuts and fitting are based on their effects on the large peak from the elastic scattering of ^{8}Li from ^{19}F nuclei in the target. Comparing the ratio of the peaks for the ^{19}F scattering before and after implementing background reduction cuts led to an estimated error of ±5% due to the energy and time gates placed on the *S*2 data. The final source of error for the *S*2 detector arises from a variation in the determined beam offset position. Varying the offset by 0.10 cm in all directions and comparing the results, a systematic error of ±4.7% from the beam offset is applied to the *S*2 data.

The errors for the data from the LEDA detector arise from similar sources as the errors for the data from the *S*2 detector; their values however, are notably different. Starting with the much lower statistics for the angular range of the LEDA detector, the statistical errors range from ±3% to ±6% and are the most significant source of error for the LEDA data. The ability to use a coincidence to separate the ^{8}Li and ^{7}Li from elastic transfer in the LEDA data from the background greatly reduced the size of the systematic errors with respect to the *S*2 data. Systematic errors due to the placement of the gates on the coincidence events in the LEDA were determined by shifting the position of the gate and comparing the results. Even with unreasonably large shifts applied to the coincidence gate the change in the results was very minimal, translating into a systematic error of only ±0.6%. The same method of varying the beam offset position as employed for the *S*2 data results in a systematic error on the LEDA data due to the beam offset of ±2.5%. This value is lower than the value for the *S*2 detector due to the rings being larger in the LEDA, and therefore less sensitive to slight offsets from the central position.

Total point-to-point errors for the *S*2 and LEDA detectors after adding the separate sources of systematic error together with the statistical errors in quadrature fall into the range of ±4% to ±7% and are summarized in Table I. The error associated with the Monte Carlo program used for determining detector geometrical coverage was included with the error values for the beam offset for each detector.

In order to calculate $S_{17}(0)$ from the ^{8}Li ANC the ratio between the mirror system overlap integrals $\langle ^{8}\mathrm{B}(2^{+})|^{7}\mathrm{Be}(\frac{3}{2}^{-})\rangle$ and $\langle ^{8}\mathrm{Li}(2^{+})|^{7}\mathrm{Li}(\frac{3}{2}^{-})\rangle$ is required. In Ref. [15], the relation between ANCs and charge symmetry breaking nucleon-nucleon (NN) interactions in mirror states was studied. Ratios between mirror ANCs were calculated using two separate effective NN potentials: the Volkov potential V2 [16] and the Minnesota (MN) potential [17]. As we know no reason to prefer one calculation over the other, average values for these ratios calculated using the two potentials of Ref. [15] are shown in Eq. (7). The error represents a systematic uncertainty meant to cover the entire range between the two calculations:

$$\begin{aligned} \frac{C^2_{p_{1/2}}(^{8}\mathrm{B})}{C^2_{p_{1/2}}(^{8}\mathrm{Li})} &= 1.22 \pm 0.03, \\ \frac{C^2_{p_{3/2}}(^{8}\mathrm{B})}{C^2_{p_{3/2}}(^{8}\mathrm{Li})} &= 1.06 \pm 0.02. \end{aligned} \tag{7}$$

Previous measurements of the ^{8}Li neutron ANC from Ref. [10] and the ^{8}B proton ANC from Ref. [18] were compared with theoretically calculated values in Ref. [15]. In both cases the experimentally determined values were much smaller than the calculated values but the ratios were in excellent agreement. Using these ratios along with experimental values for the ANCs, the *S* factor, $S_{17}(0)$, was calculated; from the V2 potential a value of $S_{17}(0) = 17.8 \pm 1.7$ eV b was obtained, and a value of 18.2 ± 1.8 eV b was obtained using the Minnesota (MN) potential [15]. These calculated values are notably smaller than but consistent with the most recent evaluation, reported by Adelberger *et al.*,

$$S_{17}(0) = 20.8 \pm 0.7(\mathrm{exp}) \pm 1.4(\mathrm{theor})\ \mathrm{eV\,b} \tag{8}$$

from Ref. [1] which is based on a mean of direct measurements.

For the current study of the ^{7}Li(^{8}Li,^{7}Li)^{8}Li reaction at 11 MeV, no optical potential for the interaction between ^{7}Li and ^{8}Li exists in the literature. Therefore, for our fits using the code FRESCO [19] the initial potential was derived from a study of ^{8}Li elastic scattering data at a laboratory energy between 13 and 20 MeV with targets in the mass range of 1 to 58 amu [20].

In order to reliably fit the large number of free parameters with the limited data set an initial fit, fixing the spectroscopic amplitudes for the $p_{1/2}$ and $p_{3/2}$ orbitals at theoretical values of 0.0737 and 0.868, respectively, from Refs. [21,22], was performed. The results of this initial fit were used as starting parameters for the optical potential in a new fit where the spectroscopic amplitude for the $p_{3/2}$ orbital was included as a fit parameter. The results from the final fit are summarized in Table II and displayed in Fig. 5. It was possible to fit the data with very high fidelity by varying the parameters within reasonable physical limits. A χ^2 value of 1.49 was obtained for

TABLE II. Values from FRESCO for the initial and final fits, for the optical potential parameters, normalization, and spectroscopic amplitude of the $p_{3/2}$ orbital, along with the associated errors of the final fit parameters.

	V (MeV)	r_V (fm)	a_V (fm)	W (MeV)	r_W (fm)	a_W (fm)	norm	$a_{3/2}$
Initial	175	0.64	0.8	16.9	1.09	0.8	9.2×10^{-3}	0.868
Final	173.8	0.500	0.957	5.28	1.514	0.531	9.35×10^{-3}	0.884
Error	2.8	0.008	0.017	0.37	0.021	0.082	0.44×10^{-3}	0.218

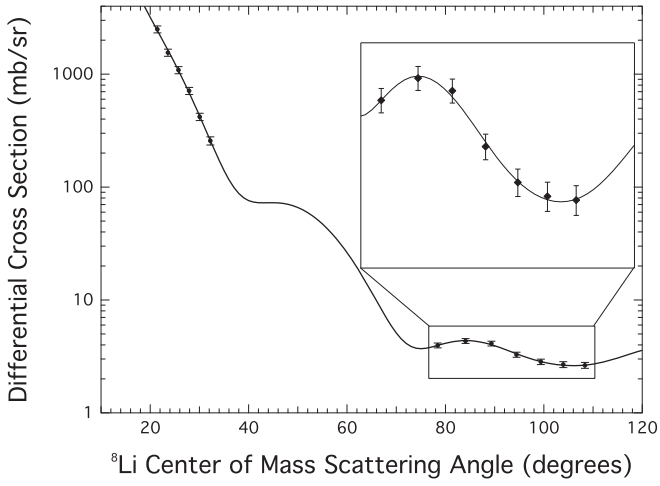

FIG. 5. Angular distribution of the ^{7}Li(^{8}Li, ^{8}Li)^{7}Li reaction at 11 MeV along with the results of the FRESCO calculation corresponding to the final parameters shown in Table II. Experimental data are shown as points with the FRESCO DWBA fit as a solid line.

13 data points and eight free parameters, which corresponds to a p value of 0.91.

It was required to add a fitting parameter for the overall normalization of the data as it could not be measured during the experiment due to unreliable readings from the channeltron used for monitoring the beam current. No significant error is expected in the ANC value on account of this problem as the absolute cross section contribution to the ANC error budget is negligible [23], with the shape rather than the magnitude of the differential cross section reflecting the ANC.

The $p_{3/2}$ spectroscopic amplitude is required twice in the FRESCO input file, once for the entrance channel and once for the exit channel. Equations (2) and (3) imply that the differential cross section is proportional to the product of the spectroscopic factors of the entrance and exit channels. Since the spectroscopic amplitudes, $A_{Yal_xj_x}$, are directly related to the spectroscopic factors by the expression

$$S_{Yal_xj_x} = |A_{Yal_xj_x}|^2, \tag{9}$$

the symmetry of the lithium transfer reaction implies that only one of the spectroscopic amplitudes for a given orbital needs to be fitted while the second may remain fixed. The results of the FRESCO fit shown in Table II give the spectroscopic amplitude for the entrance channel $p_{3/2}$ coupling value with the exit channel $p_{3/2}$ coupling value fixed at the initial value of 0.868. From these values the spectroscopic factor S, shown in Eq. (2), is calculated to be

$$S_{3/2} = 0.77 \pm 0.19. \tag{10}$$

Due to difficulties during the experiment, two additional analyses planned at distinct beam energies were not performed. The theoretical fit to the data is limited to the single data set from the 11 MeV run discussed so far. This limitation resulted in a larger error than was desired for the final extracted value of the spectroscopic amplitude.

In order to calculate the ANC from the spectroscopic factor, the squared single particle ANC given by the parameter $b^2_{p_{3/2}}(^8\text{Li})$ in Eq. (2), is required. In Ref. [24], various valence neutron binding potentials were examined for the ^{8}Li nucleus. The binding potential of Davids and Typel [25], shown as potential 1 in Table III, produced the best quality of fit of published potentials when the computed bound state wave function was compared to the variational Monte Carlo (VMC) wave function of Wiringa [21,22]. Slight variations of the parameters from the potential of Ref. [25] resulted in a new potential which produced an improved quality of fit over the original when compared to the VMC results of Wiringa. The parameters of this new binding potential are shown in Table III as potential 2.

TABLE III. Binding potentials for the $p_{3/2}$ valence neutron of ^{8}Li with corresponding squared single particle ANC values from Reference [24].

Potential #	V(MeV)	r_V(fm)	a_V(fm)	b^2(fm^{-1})	Ref.
1	43.19	2.50	0.65	0.604	[25]
2	43.53	2.50	0.60	0.560	[24]

The FRESCO fitting process previously described was performed using potential 2 from Table III. Calculating $C^2_{p_{3/2}}$ using the squared single particle ANC value of 0.560 obtained from Ref. [24] results in a value of $C^2_{3/2}(^8\text{Li}) = 0.43 \pm 0.11\,\text{fm}^{-1}$.

A study of ^{13}C(^{7}Li,^{8}Li)^{12}C at 63 MeV [10] resulted in the $p_{3/2}$ and $p_{1/2}$ ^{8}Li ANCs shown in Table IV. Of particular interest is the ratio

$$\frac{C^2_{p_{1/2}}(^8\text{Li})}{C^2_{p_{3/2}}(^8\text{Li})} = 0.13 \pm 0.02, \tag{11}$$

which was measured for the first time in that study. The error was derived from the uncertainties arising from the angular range used in the fits and uncertainties in the optical potentials.

V. RESULTS

Lacking angular coverage in this measurement that would allow separate determinations of both the $p_{1/2}$ and $p_{3/2}$ spectroscopic amplitudes, the $p_{1/2}$ ANC must be calculated from the $p_{3/2}$ ANC. The ratio between the two ANC values is taken from Ref. [10] and shown in Eq. (11). Theoretical calculations using the MN potential have also been shown to agree with this ratio [15]. Using this ratio with the calculated value for $C^2_{p_{3/2}}(^8\text{Li})$ results in $C^2_{p_{1/2}}(^8\text{Li}) = 0.056 \pm 0.016\,\text{fm}^{-1}$. The ANC values for ^{8}Li determined in this study are in agreement with those from Ref. [10] and are shown in Table IV.

Using the average of the ratio between the ^{8}Li and ^{8}B ANCs for the V2 and MN potentials from Eq. (7), the squared

TABLE IV. ^{8}Li ANC values for the $p_{3/2}$ and $p_{1/2}$ orbitals from Ref. [10] compared to values from this study.

$C^2_{p_{3/2}}(^8\text{Li})$ (fm^{-1})	$C^2_{p_{1/2}}(^8\text{Li})$ (fm^{-1})	Source
0.384 ± 0.038	0.048 ± 0.006	Ref. [10]
0.43 ± 0.11	0.056 ± 0.016	This work

^{8}B ANCs inferred from this measurement are

$$C^2_{p_{1/2}}(^8\mathrm{B}) = 0.068 \pm 0.020\,\mathrm{fm}^{-1}, \quad (12)$$

and

$$C^2_{p_{3/2}}(^8\mathrm{B}) = 0.46 \pm 0.11\,\mathrm{fm}^{-1}. \quad (13)$$

Excellent agreement is observed when comparing these results to previous measurements of Tabacaru *et al.*, $C^2_{p_{1/2}}(^8\mathrm{B}) = 0.052 \pm 0.006\,\mathrm{fm}^{-1}$ and $C^2_{p_{3/2}}(^8\mathrm{B}) = 0.414 \pm 0.043\,\mathrm{fm}^{-1}$ [9]. From the values of the ^{8}B ANCs shown in Eqs. (12) and (13) the astrophysical S factor, $S_{17}(0)$, is calculated from Eq. (6),

$$S_{17}(0) = 20.2 \pm 4.4\,\mathrm{eV\,b}. \quad (14)$$

In summary, we have for the first time inferred the ^{8}Li valence neutron ANC using the ^{7}Li(^{8}Li,^{7}Li)^{8}Li reaction. Using isospin symmetry with the measured $C^2_{p_{3/2}}(^8\mathrm{Li})$ the ^{8}B ANCs were calculated and shown to agree with previous results. $S_{17}(0)$, the astrophysical S factor for the radiative capture reaction $^7\mathrm{Be} + p \rightarrow {}^8\mathrm{B} + \gamma$, was also determined through this measurement and shown to agree with previously published values. Due to the large uncertainty, the present result is consistent with both the radiative capture measurements and the previous indirect ANC determinations, which imply a smaller value of $S_{17}(0)$. Improvements in the precision of the current result could be achieved with measurements at different ^{8}Li beam energies and at larger ^{8}Li scattering angles, both of which would help to better constrain the optical potential parameters.

ACKNOWLEDGMENTS

B.D. wishes to thank Natasha Timofeyuk for the discussions that initiated this work, which were held during a workshop at the ECT* in Trento. The authors acknowledge helpful contributions from Isao Tanihata and Sam Wright as well as the generous support of the Natural Sciences and Engineering Research Council of Canada. TRIUMF receives federal funding via a contribution agreement through the National Research Council of Canada. This work was supported by the U.S. Department of Energy, Office of Nuclear Physics, under Contract No. DE-AC02-06CH11357. The work of J.P.G. was supported by the U.S. Department of Energy, Office of Nuclear Physics, under Contract No. DE-AC02-06CH11357 and the work of I.J.T. was performed under the auspices of the U.S. Department of Energy by Lawrence Livermore National Laboratory under Contract No. DE-AC52-07NA27344 as a part of the TORUS collaboration.

[1] E. G. Adelberger *et al.*, Rev. Mod. Phys. **83**, 195 (2011).
[2] B. W. Filippone, A. J. Elwyn, C. N. Davids, and D. D. Koetke, Phys. Rev. C **28**, 2222 (1983).
[3] A. R. Junghans, K. A. Snover, E. C. Mohrmann, E. G. Adelberger, and L. Buchmann, Phys. Rev. C **81**, 012801(R) (2010).
[4] K. Abe *et al.* (Super-Kamiokande Collaboration), Phys. Rev. D **83**, 052010 (2011).
[5] P. Navrátil, R. Roth, and S. Quaglioni, Phys. Lett. B **704**, 379 (2011).
[6] J. P. Mitchell, G. V. Rogachev, E. D. Johnson, L. T. Baby, K. W. Kemper, A. M. Moro, P. N. Peplowski, A. Volya, and I. Wiedenhöver, Phys. Rev. C **82**, 011601(R) (2010).
[7] A. Azhari, V. Burjan, F. Carstoiu, H. Dejbakhsh, C. A. Gagliardi, V. Kroha, A. M. Mukhamedzhanov, L. Trache, and R. E. Tribble, Phys. Rev. Lett. **82**, 3960 (1999).
[8] A. Azhari, V. Burjan, F. Carstoiu, C. A. Gagliardi, V. Kroha, A. M. Mukhamedzhanov, X. Tang, L. Trache, and R. E. Tribble, Phys. Rev. C **60**, 055803 (1999).
[9] G. Tabacaru *et al.*, Phys. Rev. C **73**, 025808 (2006).
[10] L. Trache *et al.*, Phys. Rev. C **67**, 062801(R) (2003).
[11] A. M. Mukhamedzhanov *et al.*, Phys. Rev. C **56**, 1302 (1997).
[12] H. M. Xu, C. A. Gagliardi, R. E. Tribble, A. M. Mukhamedzhanov, and N. K. Timofeyuk, Phys. Rev. Lett. **73**, 2027 (1994).
[13] T. Davinson *et al.*, Nucl. Instrum. Methods Phys. Res. A **454**, 350 (2000).
[14] J. F. Ziegler, M. Ziegler, and J. Biersack, Nucl. Instrum. Methods Phys. Res. B **268**, 1818 (2010).
[15] N. K. Timofeyuk and P. Descouvemont, Phys. Rev. C **71**, 064305 (2005).
[16] A. Volkov, Nucl. Phys. **74**, 33 (1965).
[17] D. Thompson, M. Lemere, and Y. Tang, Nucl. Phys. A **286**, 53 (1977).
[18] A. Azhari *et al.*, Phys. Rev. C **63**, 055803 (2001).
[19] I. J. Thompson, Comput. Phys. Rep. **7**, 167 (1988).
[20] F. D. Becchetti *et al.*, Phys. Rev. C **48**, 308 (1993).
[21] R. B. Wiringa, "Two-cluster distribution functions", http://www.phy.anl.gov/theory/research/overlap/ (2011).
[22] I. Brida, S. C. Pieper, and R. B. Wiringa, Phys. Rev. C **84**, 024319 (2011).
[23] S. Burzynski *et al.*, Nucl. Phys. A **399**, 230 (1983).
[24] S. Wright, Master's thesis, University of Surrey, UK, 2006.
[25] B. Davids and S. Typel, Phys. Rev. C **68**, 045802 (2003).